19th International Conference on
Adaptive Structures and Technologies
October 6-9, 2008
Ascona, Switzerland

Coupled High-Order Layerwise Laminate Theory for Sandwich Composite Plates with Piezoelectric Actuators and Sensors

Theofanis S. Plagianakos[1]* and Dimitris A. Saravanos[2]
[1] Postdoctoral Fellow, Empa, Center for Synergetic Structures, Switzerland
Überlandstr. 129, CH-8600 Dübendorf , tel. +41448234047, fax: +41448235511, e-mail: theofanis.plagianakos@empa.ch
[2] Professor, University of Patras, Dept. of Mechanical Engineering and Aeronautics, Greece

ABSTRACT

The present paper presents a coupled high-order layerwise piezoelectric laminate theory capable of predicting both global and local electrostatic response of thick composite and sandwich composite plate structures. The through-thickness displacement field and electric potential in each discrete layer of the laminate includes quadratic and cubic polynomial approximations, in addition to the linear distributions assumed by linear layerwise theories. Stiffness, piezoelectric and permittivity matrices are formulated from ply to structural level. Interlaminar shear stress compatibility conditions are imposed on the discrete layer matrices, leading to prediction of interlaminar shear stresses at the piezoelectric-composite interfaces. A C^1 continuous finite element was implemented and modified to encompass the developed theory. Application cases include thick composite and sandwich composite plates with surface bonded piezoelectric layers acting in active and/or sensory configuration.

Keywords: piezoelectric, plate, finite element, interlaminar shear, sandwich

1. INTRODUCTION

Smart sandwich plates with composite faces and foam core and embedded piezoelectric actuators and sensors combine the superior mechanical properties of sandwich structures, such as high flexural stiffness to mass ratio, impact resistance and enhanced damping performance, with the additional capabilities to sense deformation and stress states and to adapt their response accordingly. The high thickness and inhomogeneity in properties through the thickness in both thick composite and sandwich composite structures lead to increased interlaminar shear stresses, which exhibit complex parabolic through-thickness profiles. The high shear stresses affect the global electromechanical response, but most importantly have a severe effect on the local stress field at the interface between composite and piezoelectric layers. In order to adequately capture these effects, formulation of layerwise laminate models is essential, which may yield robust predictions of the global response, but also accurate local predictions of the interlaminar and interfacial shear stresses and the deformed state of the laminate through the thickness.

The electromechanical response of smart composite structures has been extensively studied in the last two decades. Relevant reviews have been published by Saravanos and Heyliger [1], Chopra [2] for displacement-based theories and Carrera and Boscolo [3] for mixed ones. Induced strain models published in the early 90´s encompassed either single-layer [4] or linear layerwise [5]

kinematic assumptions. A coupled single-layer finite element solution for composite shells with piezoelectric layers was developed by Lammering [6], whereas Saravanos [7] developed a mixed-field shell theory by assuming linear layerwise kinematics for the electric potential. Fully linear layerwise piezoelectric beam and plate finite elements were developed by Heyliger etal [8] and Heyliger and Saravanos [9], whereas Heyliger and Brooks [10] and Heyliger [11] reported exact solutions for piezoelectric composite beams and plates, respectively. Geometrically non-linear finite element solutions based on mixed-field [12] or linear layerwise [13] kinematic assumptions were also published in the last few years. In the area of adaptive sandwich composite structures various Ritz-type [14] and exact [15] solutions, as well as, finite element formulations [16, 17, 18] assuming piecewise linear variations of the displacement and electric potential through-thickness have been published. However, linear layerwise models fail to predict interlaminar shear stress and strain at the interface between adjacent discrete layers, moreover they require a large amount of independent kinematic variables to accurately describe the through-thickness electromechanical response in thick or strongly inhomogeneous structures. To overcome these limitations some authors superimposed high-order displacement fields, globally smeared through the thickness of the laminate, on the linear approximation adopted for the displacements in each discrete layer [19, 20, 21, 22]. A few displacement-based layerwise theories have been published, which assume high-order distribution of the displacement field through the thickness of each discrete layer of the laminate. The authors developed a coupled high-order layerwise beam finite element for smart sandwich composite beams with piezoelectric actuators and sensors [23]. Zhen and Wanji [24] developed a displacement-based layerwise theory with a high-order approximation for the in plane displacements and a linear one for the electric potential in each discrete layer, and implemented a C^1-continuous triangular finite element to predict the electrostatic response of smart composite plates. Chopra and Robbins [25] published an uncoupled layerwise theory with possible quadratic through-thickness interpolation of the displacements and presented piecewise constant distributions of interlaminar shear stresses in actuated plates. Mixed high-order layerwise theories and corresponding exact solutions have been reported by D'Ottavio and Kröplin [26] and D'Ottavio, Wallmersperger and Kröplin [27] for laminated plates with piezoelectric components polarized through-thickness and shear actuators, respectively. However, although some very fine formulations are available in the literature there is a need for thorough investigation of local effects occurring in cases of practical interest, such as at the interface between adhesive and piezoelectric layer, where delaminations are probable to occur.

The objective of the current paper is to present a novel high-order theoretical framework and a corresponding finite element for predicting the coupled global and local electrostatic response of thick composite and sandwich composite plates with piezoelectric actuators and sensors. The previously published displacement-based high-order layerwise beam theory [23] is extended in plate structures with piezoelectric layers polarized through their thickness. The integrated methodology starts at the piezoelectric ply level, where constitutive equations are formulated. In the laminate level the effect of lamination and thickness is taken into account by formulation of the stiffness, piezoelectric and permittivity laminate matrices, and by imposition of interlaminar shear stress compatibility. The coupled electromechanical structural response of thick composite and sandwich composite plates is predicted by implementing a C^1-continuous finite element [28] and compared with exact [11] and Ritz-type [1] solutions.

2. THEORETICAL FORMULATION

The next paragraphs describe the integrated theoretical framework, starting from the governing material equations at the piezoelectric ply and arriving to the formulation and solution of the coupled electromechanical structural system.

2-1. Governing Material Equations

Each ply is assumed to exhibit linear piezoelectric behaviour. The constitutive equations have the form:

$$\begin{aligned} \boldsymbol{\sigma}_i &= C_{ij}^{E}\mathbf{S}_j - e_{ik}\mathbf{E}_k \\ \mathbf{D}_m &= e_{mj}\mathbf{S}_j + \varepsilon_{mk}^{S}\mathbf{E}_k \end{aligned} \tag{1}$$

where i,j=1,…,6 and k,m=1,…,3; $\boldsymbol{\sigma}_i$ and $\mathbf{S}_j$ are the mechanical stresses and engineering strains in vectorial notation; $\mathbf{E}_k$ is the electric field vector; $\mathbf{D}_m$ is the electric displacement vector; C_{ij} is the elastic stiffness tensor; e_{lk} is the piezoelectric tensor; and ε_{mk} is the electric permittivity tensor of the material. Superscripts E and S indicate constant electric field and strain conditions, respectively. The above equations may encompass the behavior of both an off-axis homogenized fibrous piezoelectric ply and a passive composite ply ([*e*]=0). The electric field vector is the gradient of the electric potential φ:

$$\mathbf{E}_k = -\partial\varphi_k / \partial x_k \qquad k=1,\ldots,3 \tag{2}$$

The current paper focuses on the prediction of the electrostatic response of multifunctional composite plate laminations containing piezoelectric materials polarized through their thickness, thus, only subscripts k,m=3 are taken into account.

2-2. Equations of Equilibrium

The variational statement of the equations of equilibrium for the piezoelectric plate is,

$$\int_A -\delta H_L \, dA + \oint_\Gamma (\delta\bar{\mathbf{u}}^T\bar{\boldsymbol{\tau}} + \delta\varphi\bar{D})\, d\Gamma = 0 \tag{3}$$

where A is the x-y surface of the beam; H_L is the electric enthalpy of the piezoelectric laminate; $\bar{\boldsymbol{\tau}}$ and $\bar{D}$ are, respectively, the surface tractions and electric displacement, acting on the boundary surface Γ; $\bar{\mathbf{u}}$ is the generalized displacement vector.

2-3. Kinematic Assumptions

A typical laminate is assumed to be subdivided into n discrete layers consisting of piezoelectric or composite material, as shown schematically in Fig. 1a. Each discrete layer may contain either a physical ply, a sublaminate, or a subply. A piecewise linear field is firstly assumed through the laminate thickness for both in-plane displacements and transverse electric potential [8], which maintains displacement continuity across the discrete layer boundaries, while allowing for different slopes in each discrete layer. Parabolic and cubic variations are superimposed on both fields through the thickness of each discrete layer (Fig. 1b). Transverse compressibility is not considered at this stage. In this context, the displacement and electric potential field in the k-th discrete layer take the form:

$$
\begin{aligned}
u^k(x,y,\zeta_k) &= U^k(x,y)\Psi_1^k(\zeta_k) + U^{k+1}(x,y)\Psi_2^k(\zeta_k) + \alpha_x^k(x,y)\Psi_3^k(\zeta_k) + \lambda_x^k(x,y)\Psi_4^k(\zeta_k)\\
v^k(x,y,\zeta_k) &= V^k(x,y)\Psi_1^k(\zeta_k) + V^{k+1}(x,y)\Psi_2^k(\zeta_k) + \alpha_y^k(x,y)\Psi_3^k(\zeta_k) + \lambda_y^k(x,y)\Psi_4^k(\zeta_k)\\
w^k(x,y,\zeta_k) &= w^o(x,y)\\
\varphi_z(x,y,\zeta_k) &= \Phi_z^k(x,y)\Psi_1^k(\zeta_k) + \Phi_z^{k+1}(x,y)\Psi_2^k(\zeta_k) + \alpha_\varphi^k(x,y)\Psi_3^k(\zeta_k) + \lambda_\varphi^k(x,y)\Psi_4^k(\zeta_k)
\end{aligned}
\tag{4}
$$

where superscripts k=1,…,n and o denote discrete layer and midplane, respectively, and ζ_k is the local thickness coordinate of layer k, defined such as ζ_k=0 at the middle of the discrete layer, ζ_k=1 and ζ_k=-1 at the top and the bottom, respectively, of the discrete layer k. Thus, the first two terms on the right hand side of the approximations of the in-plane displacements and electric potential describe the linear field; U^k, V^k, U^{k+1}, V^{k+1} and Φ_z^k, Φ_z^{k+1} are the respective values at bottom and top of the discrete layer, effectively describing extension and rotation, and electric potential at the terminals, respectively, of the layer [8].The last two terms describe quadratic and cubic variations of the in-plane displacements and electric potential and vanish at top and bottom of the discrete layer, since the polynomial functions Ψ_3^k and Ψ_4^k have been selected to ensure displacement continuity across the discrete layer boundaries,

$$
\begin{aligned}
\Psi_1^k &= (1-\zeta_k)/2\\
\Psi_2^k &= (1+\zeta_k)/2\\
\Psi_3^k &= \frac{h_k}{2}(\zeta_k^2-1)\\
\Psi_4^k &= \frac{h_k}{2}\zeta_k(\zeta_k^2-1)
\end{aligned}
\tag{5}
$$

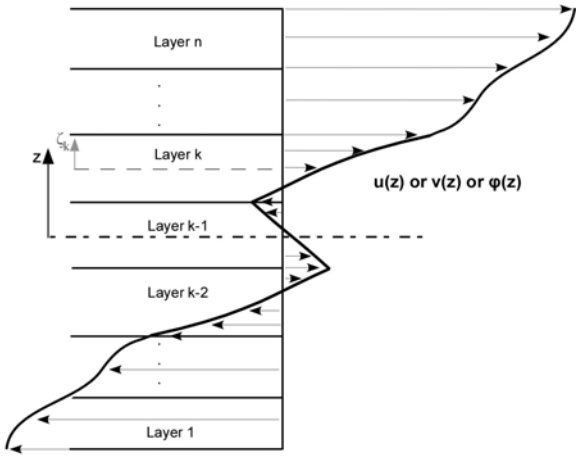

(a)

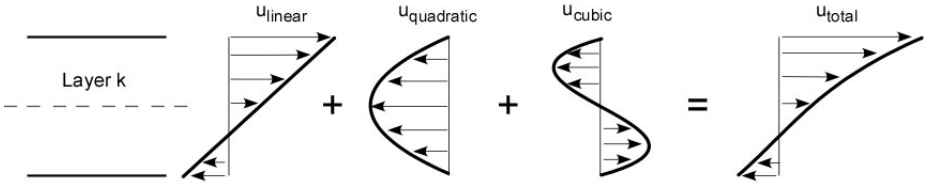

(b)

Figure 1. Schematic representation of the high-order layerwise laminate theory in a typical laminate configuration analyzed with n-discrete layers. a) Kimematic approximation through the thickness for the in-plane displacements and electric potential, b) Assumed field components through the thickness of a discrete layer; the linear component corresponds to a linear layerwise model.

The high-order terms α_x^k, α_y^k and λ_x^k, λ_x^k in eq. (4) may be described as "hyper-rotations" of each discrete layer introduced by the quadratic and cubic polynomials, respectively. The present model distinguishes in this point from high-order approximations globally smeared through the laminate thickness, since the high-order terms are additional degrees of freedom of the discrete layer. The same applies also for the high-order electric potential terms α_φ^k, λ_φ^k.

2-4. Through-Thickness Strain and Electric Field

In the context of the kinematic assumptions (3), the interlaminar shear strains S_4 and S_5 take the form:

$$\begin{aligned} S_4^k &= w_{,y}^o + \frac{V^{k+1} - V^k}{h_k} + 2\zeta_k \alpha_y^k + (3\zeta_k^2 - 1)\lambda_y^k \\ S_5^k &= w_{,x}^o + \frac{U^{k+1} - U^k}{h_k} + 2\zeta_k \alpha_x^k + (3\zeta_k^2 - 1)\lambda_x^k \end{aligned} \tag{6}$$

The comma in the subscripts indicates differentiation. The first two right hand side terms yield a constant shear term, while the last two terms provide a linear and a quadratic distribution through the thickness of the k-th layer. The in-plane strains are expressed as

$$\begin{aligned} S_1^k &= U_{,x}^k \Psi_1^k + U_{,x}^{k+1} \Psi_2^k + \alpha_{x,x}^k \Psi_3^k + \lambda_{x,x}^k \Psi_4^k \\ S_2^k &= V_{,y}^k \Psi_1^k + V_{,y}^{k+1} \Psi_2^k + \alpha_{y,y}^k \Psi_3^k + \lambda_{y,y}^k \Psi_4^k \\ S_{6a}^k &= U_{,y}^k \Psi_1^k + U_{,y}^{k+1} \Psi_2^k + \alpha_{x,y}^k \Psi_3^k + \lambda_{x,y}^k \Psi_4^k \\ S_{6b}^k &= V_{,x}^k \Psi_1^k + V_{,x}^{k+1} \Psi_2^k + \alpha_{y,x}^k \Psi_3^k + \lambda_{y,x}^k \Psi_4^k \end{aligned} \tag{7}$$

The electric field in the poling direction is derived by combining eqs. (2) and (4),

$$\mathbf{E}_3^k = -(\Phi_z^k \Psi_{1,\zeta_k}^k + \Phi_z^{k+1} \Psi_{2,\zeta_k}^k + \alpha_\varphi^k \Psi_{3,\zeta_k}^k + \lambda_\varphi^k \Psi_{4,\zeta_k}^k) \frac{2}{h_k} \tag{8}$$

and accounts for a quadratic through-thickness profile in each discrete layer.

2-5. Laminate Electric Enthalpy and Laminate Matrices

The electric enthalpy of the piezocomposite laminate is:

$$\delta H_L = \sum_{k=1}^{n} \begin{bmatrix} \left(\delta \mathbf{S}^k\right)^T \left[\mathbf{Q}^k\right] \mathbf{S}^k + \left(\delta \mathbf{S}_s^k\right)^T \left[\mathbf{Q}_s^k\right] \mathbf{S}_s^k - \left(\delta \mathbf{S}^k\right)^T \left[\boldsymbol{P}^k\right] \mathbf{E}_3^k \\ -\left(\delta \mathbf{E}_3^k\right)^T \left[\boldsymbol{P}^k\right]^T \left(\delta \mathbf{S}^k\right) - \left(\delta \mathbf{E}_3^k\right)^T \left[\boldsymbol{L}^k\right] \mathbf{E}_3^k \end{bmatrix} \tag{9}$$

where k=1,…,n are the discrete layers of the laminate, $\left[\mathbf{Q}^k\right]$ (dimension 16x16) and $\left[\mathbf{Q}_s^k\right]$ (dimension 10x10) are the in-plane and interlaminar shear stiffness matrices, respectively, of the

discrete layer [29] and $\mathbf{S}^k$ and $\mathbf{S}_s^k$ are the in-plane and interlaminar shear strain vectors, respectively, of the discrete layer given by,

$$\begin{aligned}\mathbf{S}^k &= \left\{ \begin{matrix} U^k_{,x}, U^{k+1}_{,x}, V^k_{,y}, V^{k+1}_{,y}, U^k_{,y}, U^{k+1}_{,y}, V^k_{,x}, V^{k+1}_{,x}, \\ \alpha^k_{x,x}, \alpha^k_{y,y}, \alpha^k_{x,y}, \alpha^k_{y,x}, \lambda^k_{x,x}, \lambda^k_{y,y}, \lambda^k_{x,y}, \lambda^k_{y,x} \end{matrix} \right\} \\ \mathbf{S}_s^k &= \left\{ w^o_{,y}, V^k, V^{k+1}, w^o_{,x}, U^k, U^{k+1}, \alpha^k_y, \alpha^k_x, \lambda^k_y, \lambda^k_x \right\}\end{aligned} \tag{10}$$

$\left[\boldsymbol{P}^k \right]$ (dimension 16x4) and $\left[\boldsymbol{L}^k \right]$ (dimension 4x4) are the piezoelectric and electric permittivity layer matrices, respectively, given by

$$\left[\boldsymbol{P}^{(k)} \right] = \begin{bmatrix} \boldsymbol{P}^{i(k)}_{ll} & \boldsymbol{P}^{i(k)}_{lq} & \boldsymbol{P}^{i(k)}_{lc} \\ \boldsymbol{P}^{i(k)}_{ql} & \boldsymbol{P}^{i(k)}_{qq} & \boldsymbol{P}^{i(k)}_{qc} \\ \boldsymbol{P}^{i(k)}_{cl} & \boldsymbol{P}^{i(k)}_{cq} & \boldsymbol{P}^{i(k)}_{cc} \end{bmatrix} \tag{11}$$

$$\left[\boldsymbol{L}^{(k)} \right] = \begin{bmatrix} \boldsymbol{L}^{i(k)}_{ll} & \boldsymbol{L}^{i(k)}_{lq} & \boldsymbol{L}^{i(k)}_{lc} \\ & \boldsymbol{L}^{i(k)}_{qq} & \boldsymbol{L}^{i(k)}_{qc} \\ & & \boldsymbol{L}^{i(k)}_{cc} \end{bmatrix} \tag{12}$$

where i=1,2. As seen in eq. (10) the piezoelectric laminate matrix is not symmetric. The respective submatrices for both piezoelectric and permittivity matrices are formulated by taking into account eqs. (1), (7) and (8) and are shown in the Appendix.

2-6. Through-Thickness Shear Stress Compatibility

Combination of interlaminar shear strains in eq. (4) with Hooke´s law yield a quadratic shear stress field through the thickness of a discrete layer. The through-thickness continuity of the interlaminar shear stresses between adjacent layers is weakly maintained through the equations of equilibrium (3) (Fig. 2a). To further ensure shear stress continuity, compatibility equations were explicitly imposed. The interlaminar shear stresses should be continuous between adjacent layers (eqs. 13b) and vanish at the top and bottom of the plate for traction free surfaces (eqs. 13a and c),

$$\begin{aligned} &\sigma^1_4(\zeta_1 = -1) = \sigma^1_5(\zeta_1 = -1) = 0 && && \text{(a)} \\ &\sigma^k_4(\zeta_k = 1) = \sigma^{k+1}_4(\zeta_{k+1} = -1) && \text{k=1,...,n-1} && \text{(b)} \\ &\sigma^k_5(\zeta_k = 1) = \sigma^{k+1}_5(\zeta_{k+1} = -1) && && \\ &\sigma^n_4(\zeta_n = 1) = \sigma^n_5(\zeta_n = 1) = 0 && && \text{(c)} \end{aligned} \tag{13}$$

The imposition of equations (13) combined with the high-order approximation of the displacement field variables (4) enables prediction of compatible interlaminar shear stresses through the thickness of the plate by using a minimum number of discrete layers. Moreover, 2n+2 hyper-rotations of the composite laminate, namely all λ_y, λ_x and the α_y, α_x of the top discrete layer are eliminated, while the remaining elastic variables of the discrete layers get coupled,

$$\begin{Bmatrix}\lambda_y^k\\ \lambda_x^k\end{Bmatrix}=\left[\tilde{\Lambda}^{(k,k)}\right]\Xi_s^k+\left[\tilde{\Lambda}^{(k,k-1)}\right]\Xi_s^{k-1}+\ldots+\left[\tilde{\Lambda}^{(k,1)}\right]\Xi_s^1 \qquad \text{(a)}$$

$$\begin{Bmatrix}\alpha_y^n\\ \alpha_x^n\end{Bmatrix}=\left[\hat{\Lambda}^{(n,n)}\right]\begin{Bmatrix}\Xi_s^{*n}\\ \lambda_y^n\\ \lambda_x^n\end{Bmatrix} \qquad k=1,\ldots,n-1 \qquad \text{(b)} \qquad (14)$$

$$\begin{Bmatrix}\lambda_y^n\\ \lambda_x^n\end{Bmatrix}=\left[\tilde{\Lambda}^{*(n,n)}\right]\Xi_s^{*n}+\left[\tilde{\Lambda}^{(n,n-1)}\right]\Xi_s^{n-1}+\ldots+\left[\tilde{\Lambda}^{(n,1)}\right]\Xi_s^1 \qquad \text{(c)}$$

where $\tilde{\Lambda},\hat{\Lambda},\tilde{\Lambda}^*$ are reduction matrices arising from the rearrangement of eqs. (13), and their superscript (k,m with m≤k) indicates the expression of hyper-rotations of layer k as a function of the interlaminar shear vector of layer m [29]; Ξ_s^k, Ξ_s^{*n} are vectors containing interlaminar shear variables of layers k and n, respectively, given by

$$\Xi_s^k=\left\{w_{,y}^o,V^k,V^{k+1},w_{,x}^o,U^k,U^{k+1},\alpha_y^k,\alpha_x^k\right\}$$
$$\Xi_s^{*n}=\left\{w_{,y}^o,V^n,V^{n+1},w_{,x}^o,U^n,U^{n+1}\right\} \qquad k=1,\ldots,n-1 \qquad (15)$$

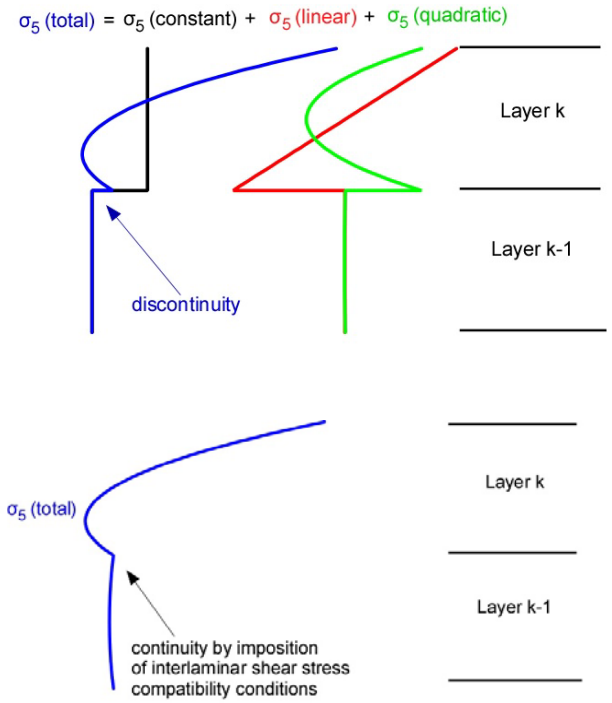

(a)

(b)

Figure 2. Effect of interlaminar shear stress compatibility imposition: a) Discontinuous distribution of interlaminar shear stress σ_5 through the thickness of two adjacent disceret layers in the case that no compatibility conditions are imposed, b) Continuous interlaminar shear stress distribution by imposition of compatibility conditions.

The elimination of respective high-order in-plane elastic variables involves similar strain vectors

$$
\begin{aligned}
\Xi_x^k &= \left\{ w^o_{,yx}, V^k_{,x}, V^{k+1}_{,x}, w^o_{,xx}, U^k_{,x}, U^{k+1}_{,x}, \alpha^k_{y,x}, \alpha^k_{x,x} \right\} \\
\Xi_y^k &= \left\{ w^o_{,yy}, V^k_{,y}, V^{k+1}_{,y}, w^o_{,xy}, U^k_{,y}, U^{k+1}_{,y}, \alpha^k_{y,y}, \alpha^k_{x,y} \right\} \\
\Xi_x^{*n} &= \left\{ w^o_{,yx}, V^n_{,x}, V^{n+1}_{,x}, w^o_{,xx}, U^n_{,x}, U^{n+1}_{,x} \right\} \\
\Xi_y^{*n} &= \left\{ w^o_{,yy}, V^n_{,y}, V^{n+1}_{,y}, w^o_{,xy}, U^n_{,y}, U^{n+1}_{,y} \right\}
\end{aligned}
\qquad k=1,\ldots,n-1 \qquad (16)
$$

which yield the requirement of a C^1-continuous transverse displacement approximation in the x-y plane. The reduced stiffness and piezoelectric laminate matrices arise from static condensation and are shown in the Appendix.

2-7. Finite Element Implementation

A C^1-continuous finite element [28] was modified to include electric degrees of freedom. The generalized state variables in the element were approximated as,

$$
\begin{aligned}
w^o(\xi,\eta) &= \sum_{i=1}^{4} \left(\begin{array}{l} w^{o(i)} H_1^{(i)}(\xi,\eta) + \dfrac{L_{xe}}{2} w^{o(i)}_{,x} H_2^{i}(\xi,\eta) + \dfrac{L_{ye}}{2} w^{o(i)}_{,y} H_3^{i}(\xi,\eta) \\ + \dfrac{L_{xe} L_{ye}}{4} w^{o(i)}_{,xy} H_4^{i}(\xi,\eta) \end{array} \right) \\
U^k(\xi,\eta) &= \sum_{i=1}^{4} U^{k(i)} N^{(i)}(\xi,\eta) \\
V^k(\xi,\eta) &= \sum_{i=1}^{4} V^{k(i)} N^{(i)}(\xi,\eta) \\
\alpha_x^l(\xi,\eta) &= \sum_{i=1}^{4} \alpha_x^{l(i)} N^{(i)}(\xi,\eta) \\
\alpha_y^l(\xi,\eta) &= \sum_{i=1}^{4} \alpha_y^{l(i)} N^{(i)}(\xi,\eta) \\
\Phi_z^k(x) &= \sum_{i=1}^{L} \Phi_z^{ki} N^i(x) \\
\alpha_\varphi^m(x) &= \sum_{i=1}^{L} \alpha_\varphi^{mi} N^i(x) \\
\lambda_\varphi^m(x) &= \sum_{i=1}^{L} \lambda_\varphi^{mi} N^i(x)
\end{aligned}
\qquad (17)
$$

where k=1,…,n+1, l=1,…,n-1, m=1,…,n; ξ and η are the element local coordinates and i denotes finite element node; H are 2-D Hermitian polynomials [30] and N are linear shape functions. Thus, the current finite element has 7n+5 nodal degrees of freedom.

2-8. Coupled Piezoelectric Structural System

Combination of Eqs. (15-17) with the expressions of the reduced laminate matrices and substitution into the governing equations of equilibrium (3) leads to the formulation of the coupled piezoelectric system in discrete matrix form:

$$\begin{bmatrix} [K_{uu}] & [K_{u\varphi}^{FF}] \\ [K_{\varphi u}^{FF}] & [K_{\varphi\varphi}^{FF}] \end{bmatrix} \begin{Bmatrix} \{\bar{\mathbf{u}}\} \\ \{\boldsymbol{\varphi}^{F}\} \end{Bmatrix} = \begin{Bmatrix} \{\mathbf{P}\} - [K_{u\varphi}^{FA}]\{\boldsymbol{\varphi}^{A}\} \\ \{\mathbf{Q}^{F}\} - [K_{\varphi\varphi}^{FA}]\{\boldsymbol{\varphi}^{A}\} \end{Bmatrix} \tag{18}$$

Submatrices $[K_{uu}]$, $[K_{u\varphi}]$ and $[K_{\varphi\varphi}]$ indicate the elastic, piezoelectric and permittivity matrices of the structure; superscripts F and A indicate, respectively, sensory (free) and active (applied) electric potential components; $\{\mathbf{P}\}$ is the applied mechanical force vector and $\{\mathbf{Q}^{F}\}$ is the applied electric charge at the sensors. Solution of the above system yields the coupled electrostatic response of the piezoelectric plate in active or/and sensory configuration.

3. APPLICATION CASES

The present methodology (HLPT) was validated with an exact solution [11] and a linear layerwise Ritz-type exact solution [1] (LLPT) for a benchmark thick composite plate. Predictions of the mixed-field piezoelectric theory [7] (FSPT), which models the elastic field by a single-layer, were also addressed in the validation studies. Further case studies included the sensory response of a cantilever thick composite beam and of a sandwich composite plate. The materials considered are listed in Table 1.

Table 1. Electromechanical properties of materials considered.

Material	Gr/Epoxy(1)	Gr/Epoxy(2)	Adhesive	Foam	Pzt-4
Elastic Properties					
E_{11} (GPa)	132.4	126.0	6.9	0.049	81.3
E_{22} (GPa)	10.8	7.9	6.9	0.049	81.3
E_{33} (GPa)	10.8	7.9	6.9	0.049	64.5
G_{12} (GPa)	5.7	3.4	2.5	0.0152	30.6
G_{13} (GPa)	5.7	3.4	2.5	0.0152	25.6
G_{23} (GPa)	3.6	2.0	2.5	0.0152	25.6
v_{12}	0.24	0.28	0.40	0.42	0.329
v_{13}	0.24	0.28	0.40	0.42	0.432
v_{23}	0.40	0.40	0.40	0.42	0.432
Piezoelectric Properties					
d_{31} (10^{-12} m/V)	0.08	0.65	1.60	1.59	1.59
d_{32} (10^{-12} m/V)	0.67	1.70	1.60	1.59	1.59
Dielectric Properties (ε_0=8.85 10^{-12} farad/m)					
$\varepsilon_{33}/\varepsilon_0$	3.0	3.0	3.0	3.0	1475

3-1. [Pzt-4/0/90]$_s$ Plate

A square simply-supported cross-ply thick (a/h=4) composite plate with Graphite/Epoxy[1] plies and two piezoelectric layers [1] was studied. Two configurations were considered: 1) a double sensory configuration, where a doubly sinusoidal pressure of amplitude 1kPa was applied and 2) an active-sensory configuration, where a doubly sinusoidal electric potential of amplitude 200 Volt was applied at the inner terminal of the lower piezoelectric layer. In both cases the outer surfaces of the piezoelectric layers were grounded. A 10x10 uniform finite element mesh was used for the quarter model addressing 5 discrete layers in the case of the HLPT, whereas 24 layers were applied in the case of the LLPT.

Figs 3a and b show predicted deflection and electric potential, respectively, through the thickness of the plate in the points of their maximum values. Both are normalized according to [1].

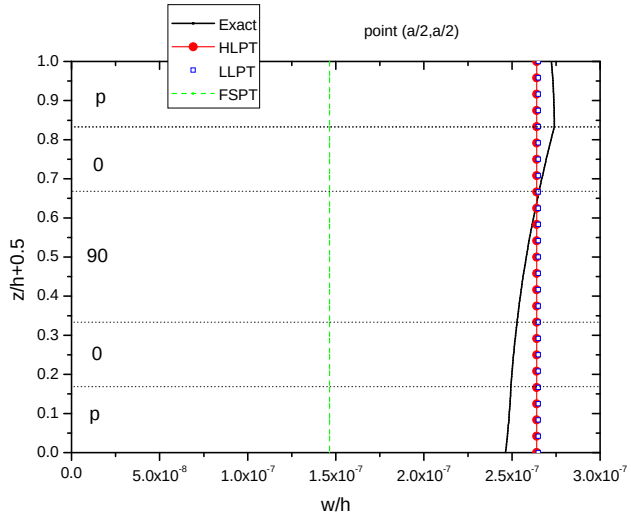

(a)

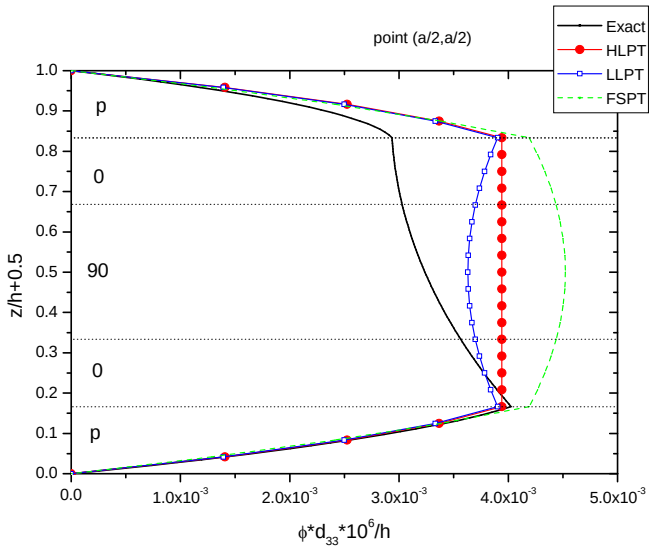

(b)

Figure 3. Through-thickness distribution of transverse displacement and electric potential, respectively, in a thick double sensory cross ply plate. The symbols indicate prediction points.

The present theory correlates well with the linear layerwise formulation for the transverse

displacement, whereas the small deviation to the exact solution is attributed to transverse compressibility and the d_{33} piezoelectric effect, which both layerwise models neglect. These effects are dominant in the electric potential distribution. The electric potential in the composite layers is caused by their electric permittivity. Both LLPT and exact solution take into account permittivity in all directions, whereas only through-thickness permittivity is considered in the present model. Thus, the variation of the electric potential predicted by both LLPT and exact solutions has a parabolic form in the composite layers. The transverse out of plane effects smoothen in the active/sensory case as seen in Figs. 4a and b.

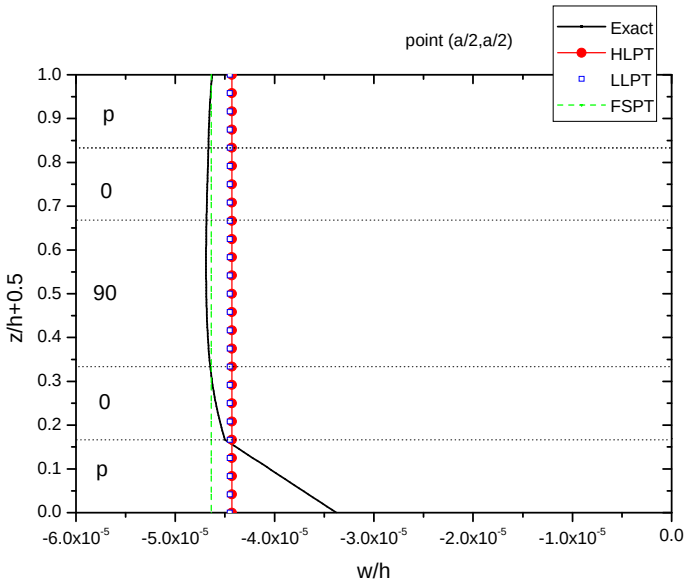

(a)

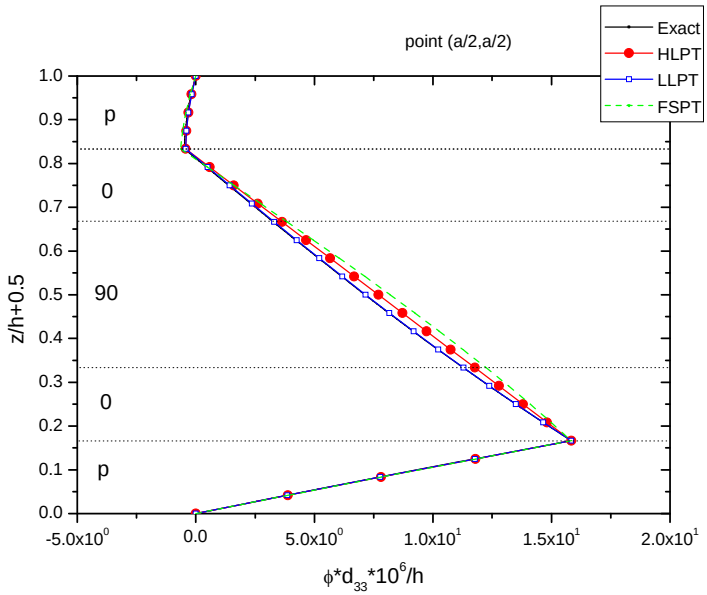

(b)

Figure 4. Through-thickness distribution of transverse displacement and electric potential, respectively, in a thick active-sensory cross ply plate. The symbols indicate prediction points.

Figs. 5a and b present through-thickness distributions of normalized interlaminar shear

stresses in the points of their maximum values.

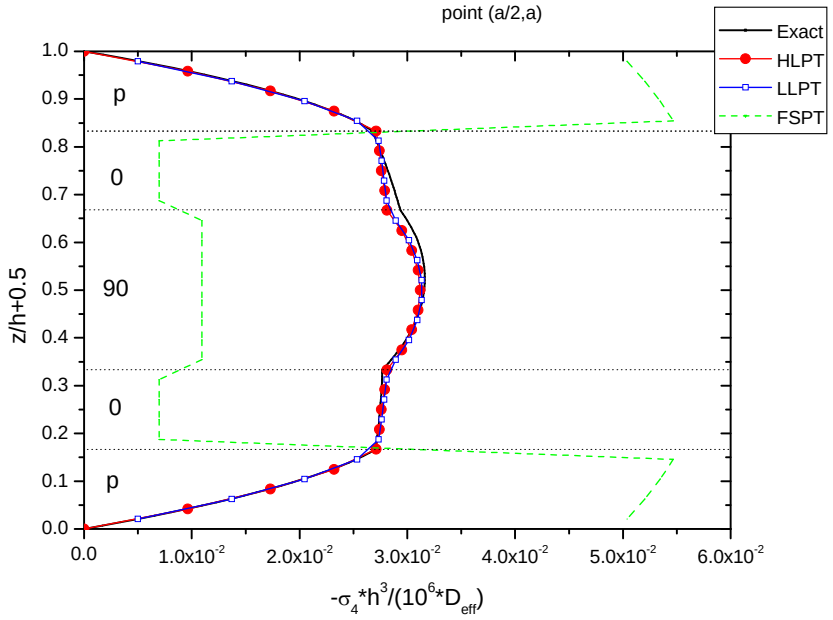

(a)

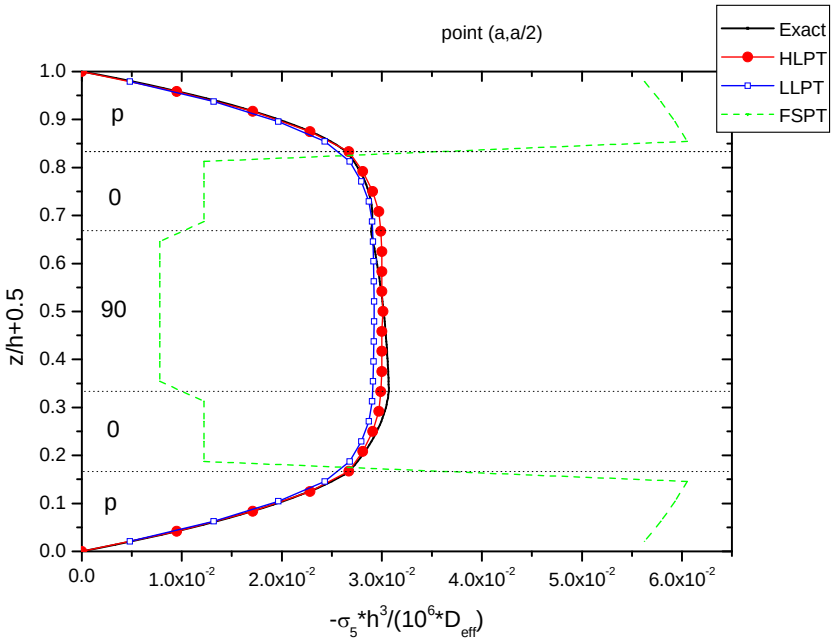

(b)

Figure 5. Through-thickness distributions of interlaminar shear stresses in a thick double sensory cross ply plate.

The current solution captures the interlaminar shear response both accurately and efficiently using a minimum number of discrete layers. Moreover, it predicts interlaminar shear stress at the interfaces between the discrete layers, whereas the LLT gives prediction at the middle of each layer and needs refinement to capture the interface response. This key-feature of the current mechanics is more clearly illustrated in the active-sensory case (Figs. 6a and b).

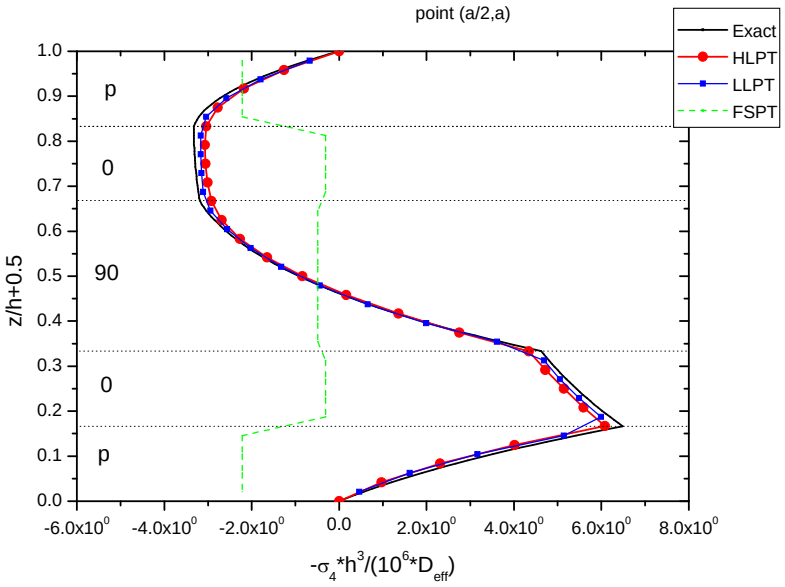

(a)

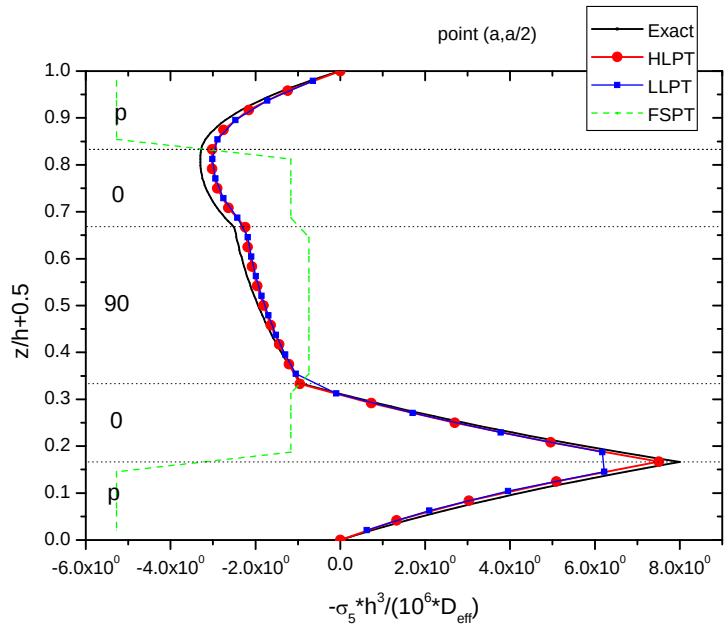

(b)

Figure 6. Through-thickness distributions of interlaminar shear stresses in a thick active-sensory cross ply plate.

3-2. [0/Adhesive/Pzt-4] beam

The case of a cantilever thick (a/h=9) Graphite/Epoxy[2] beam with a piezoelectric layer [9] bonded on the upper surface by an adhesive layer highlights the capabilities of the developed laminate mechanics. A 25x2 FE mesh and 3 discrete layers through the thickness were used to model the beam. The electrostatic response is predicted for both active and sensory configuration. In the sensory case a transverse load of 1 kN was applied at the tip, while in the active case a uniform potential of 12.5 kVolt was considered to act on the outer surface. Fig. 7a illustrates the distribution of interlaminar shear stress at the interface between piezoelectric and adhesive layer in the x-y plane for

the active configuration. It can be observed that maximum shear stresses appear near the tip of the beam. The through-thickness distribution of interlaminar shear stress near the tip is shown in Fig. 7b. It yields parabolic profiles, which are efficiently captured by the present solution.

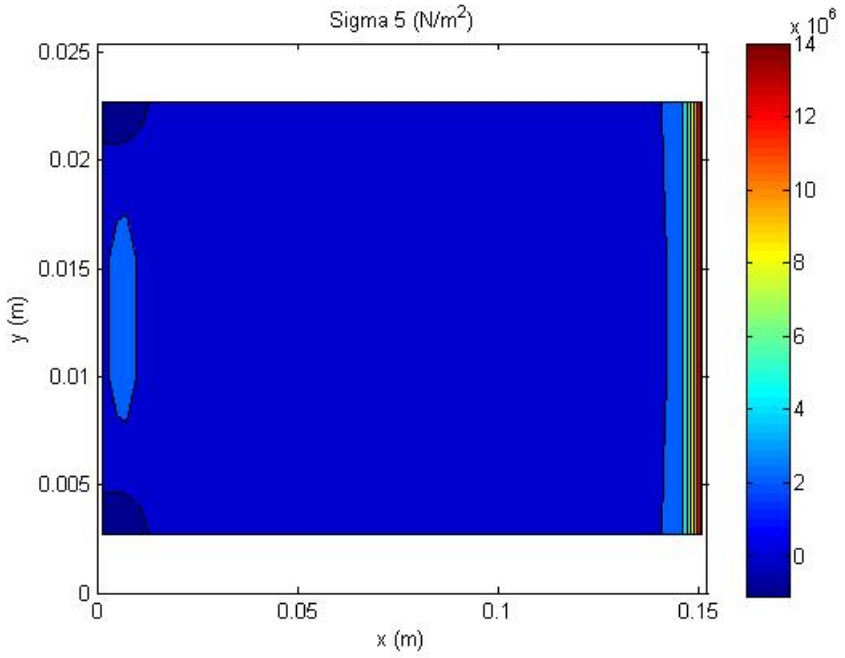

(a)

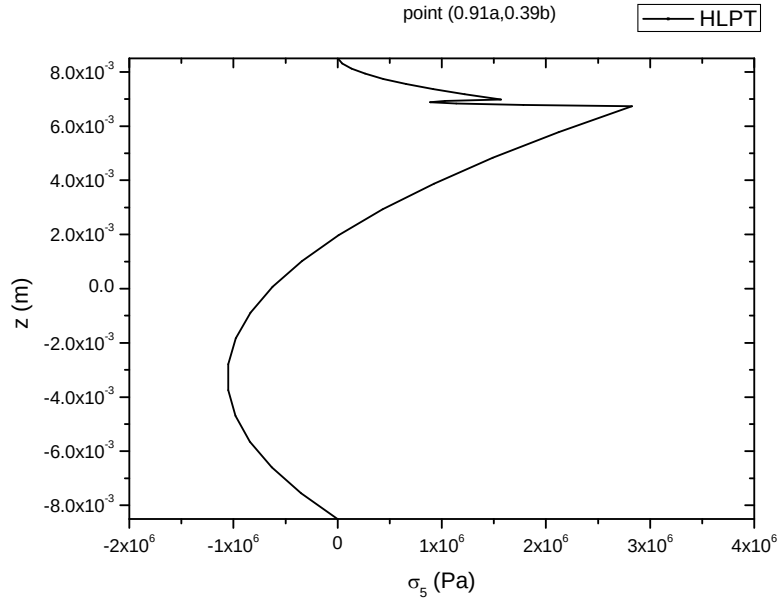

(b)

Figure 7. Distribution of interlaminar shear stress in an active thick composite beam. a) Interfacial stress between adhesive-piezoelectric layers along plane, b) Through-thickness distribution.

In the sensory case maximum interlaminar shearing between Pzt-4/Adhesive layers occur near the support (Fig. 8a) and is probably affected by edge effects. The distribution of σ_5 near the middle of the beam is plotted in Fig. 8b and also exhibits a parabolic form.

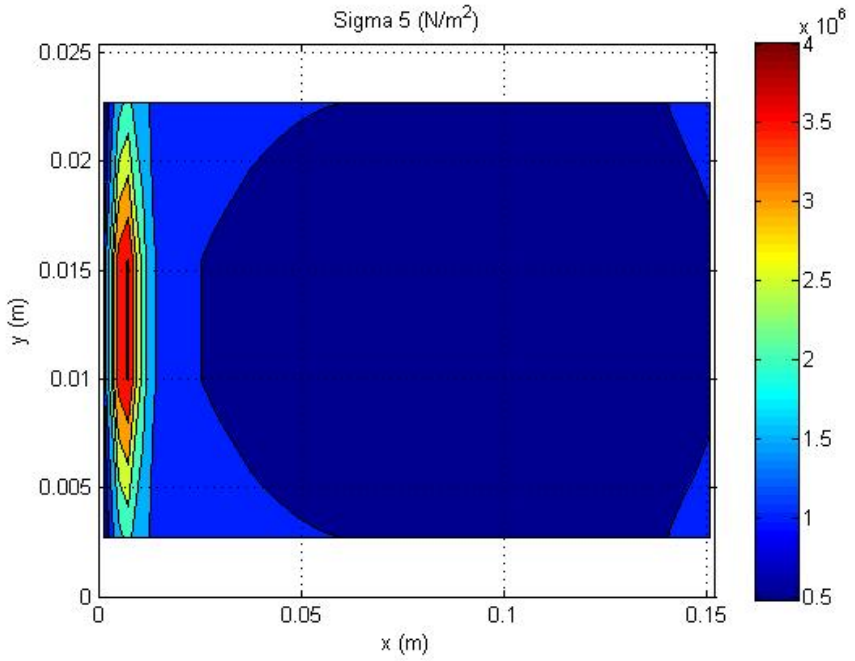

(a)

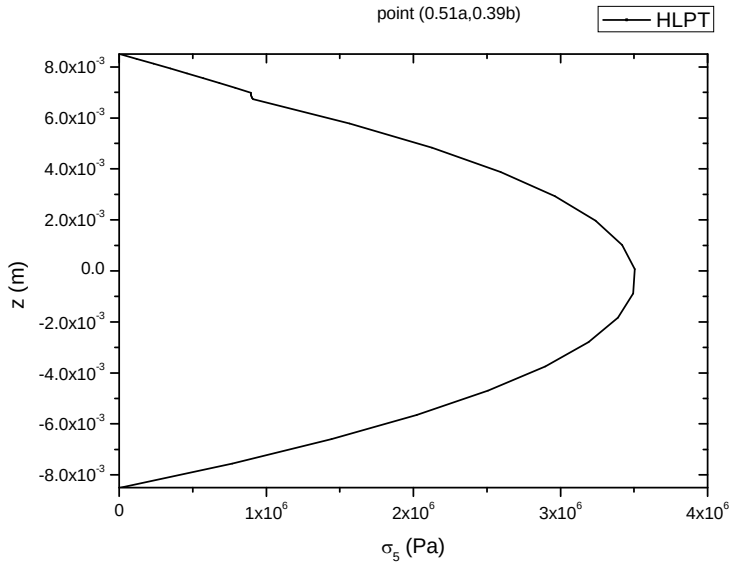

(b)

Figure 8. Distribution of interlaminar shear stress in a sensory thick composite beam. a) Interfacial stress between adhesive-piezoelectric layers along plane, b) Through-thickness distribution.

3-3. [0/foam/0/Adhesive/Pzt-4] Sandwich Composite Plate

A moderately thick (a/h=25) simply-supported sandwich plate consisting of Graphite/Epoxy[2] composite faces, foam core and a piezoelectric sensory layer adhesively bonded at the upper surface was studied. The plate was subjected to a constant pressure of 1kPa and the outer face of the piezoelectric layer was grounded. A 10x10 uniform finite element mesh and 5 discrete layers were used to model one quarter of the plate. Figs. 9a, 10a illustrate predicted in-plane distributions of the current solution for the interlaminar shear stress σ_4, σ_5 respectively, at the interface between adhesive-piezoelectric layers.

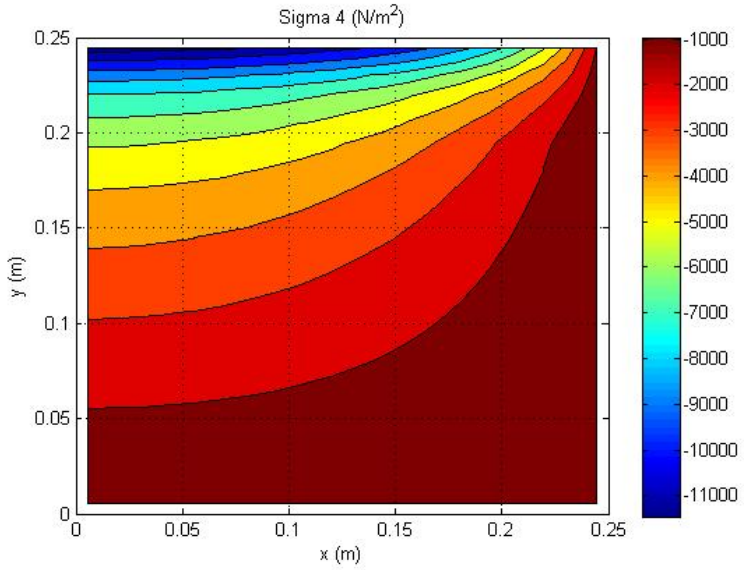

(a)

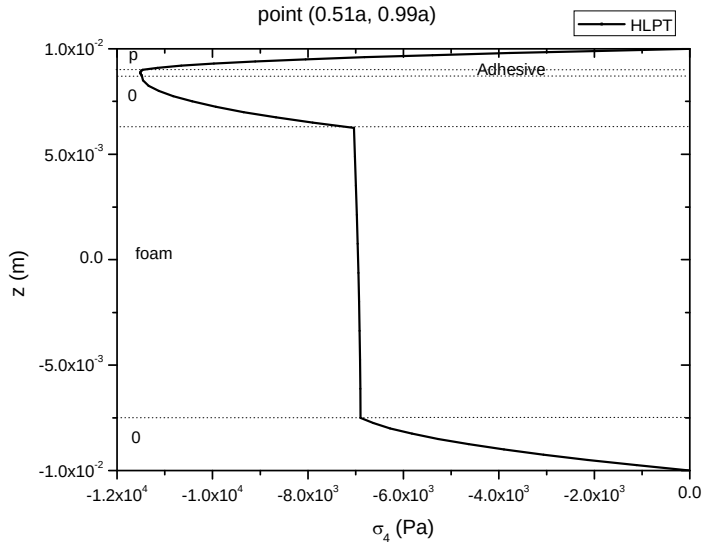

(b)

Figure 9. Distribution of interlaminar shear stress σ_4 in a sensory sandwich composite plate. a) Interfacial stress between adhesive-piezoelectric layers along plane, b) Through-thickness distribution.

The predicted distributions of interlaminar shear stresses through the thickness of the plate are shown in Figs. 9b and 10b respectively. The parabolic distributions observed can be efficiently captured by the present methodology.

3. SUMMARY

A high-order layerwise piezoelectric plate theory and a corresponding finite element were presented. The theory enables accurate prediction of the coupled global and local electrostatic response of thick composite and sandwich composite plates. Its major contributions lie on the accuracy and efficiency in capturing interlaminar shear effects through the thickness, as well as, on the prediction of interlaminar shear stress at the interface between composite and piezoelectric layers. The latter is crucial information for predicting delamination initiation in strongly inhomogeneous

laminations, as the ones studied in this work. Future studies will focus on the inclusion of transverse compressibility in the developed mechanics and experimental validation in composite and sandwich composite plates with piezoelectric patches.

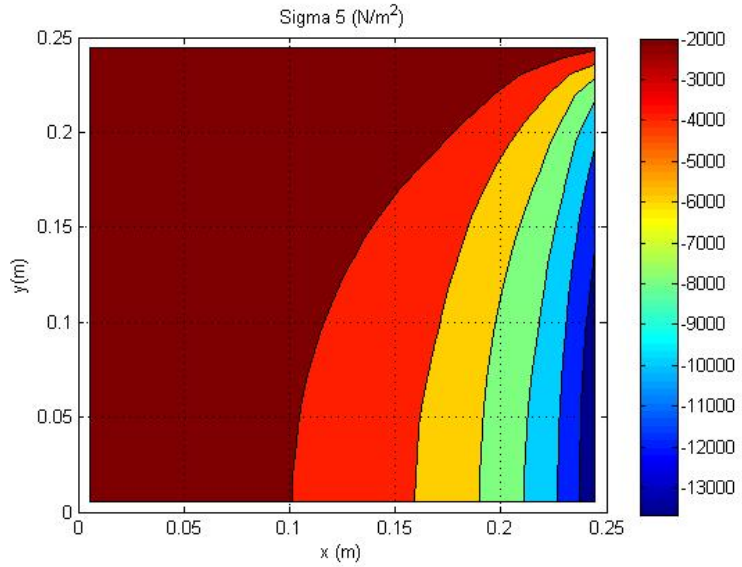

(a)

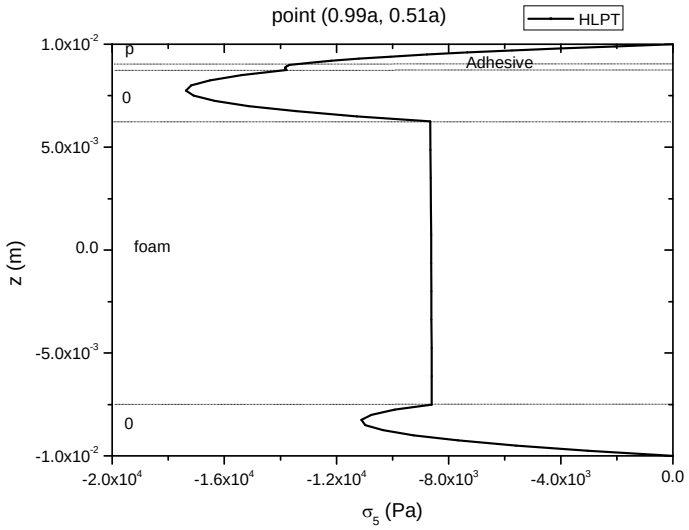

(b)

Figure 10. Distribution of interlaminar shear stress σ_5 in a sensory sandwich composite plate. a) Interfacial stress between adhesive-piezoelectric layers along plane, b) Through-thickness distribution.

REFERENCES

1. Saravanos, D. A. and P. R. Heyliger, "Mechanics and Computational Models for Laminated Piezoelectric Beams, Plates and Shells," *ASME Applied Mechanics Reviews*, Vol. 52, pp. 305-320 (October 1999).
2. Chopra, I., "Review of State of Art of Smart Structures and Integrated Systems," *AIAA Journal*, Vol. 40, pp. 2145-2187 (November 2002).
3. Carrera, E. and M. Boscolo, "Classical and Mixed Finite Elements for Static and Dynamic Analysis of Piezoelectric Plates," *International Journal for Numerical Methods in Engineering*,

Vol. 70, pp. 1135-1181 (June 2007).
4. Crawley, E. F. and K. B. Lazarus, "Induced Strain Actuation of Isotropic and Anisotropic Plates," *AIAA Journal*, Vol. 29, pp. 944-951 (June 1991).
5. Robbins, D. H. and J. N. Reddy, "Analysis of Piezoelectrically Actuated Beams Using a Layerwise Displacement Theory," *Computers & Structures*, Vol. 41, pp. 265-279 (1991).
6. Lammering, R., "The application of a shell finite element for composites containing piezoelectric polymers in vibration control," *Computers & Structures*, Vol. 41, pp. 1101-1109 (1991).
7. Saravanos, D. A., "Coupled Mixed-Field Laminate Theory and Finite Element for Smart Piezoelectric Composite Structures," *AIAA Journal*, Vol. 35, pp. 1327-1333 (August 1997).
8. Heyliger, P. R., G. Ramirez, and D. A. Saravanos, "Coupled Discrete-Layer Finite-Element Models for Laminated Piezoelectric Plates," *Communications in Numerical Methods in Engineering*, Vol. 10, pp. 971-981 (December 1994).
9. Saravanos, D. A. and P. R. Heyliger, "Coupled Layerwise Analysis of Composite Beams with Embedded Piezoelectric Sensors and Actuators," *Journal of Intelligent Material Systems and Structures*, Vol. 6, pp. 350-363 (May 1995).
10. Heyliger, P. R. and S. P. Brooks, "Exact Solutions for Piezoelectric Laminates in Cylindrical Bending" *Journal of Applied Mechanics*, Vol. 63, pp. 903-910 (December 1996).
11. Heyliger, P. R., "Exact Solutions for Simply-Supported Laminated Piezoelectric Plates," *Journal of Applied Mechanics*, Vol. 64, pp. 299-306 (June 1997).
12. Varelis, D. and D. A. Saravanos, "Coupled Buckling and Postbuckling Analysis of Active Laminated Piezoelectric Composite Plates," *International Journal of Solids and Structures*, Vol. 41, pp. 1519-1538 (March 2004).
13. Giannopoulos, G., F. Santafe, J. Monreal, and J. Vantomme, "Thermal, Electrical, Mechanical Coupled Mechanics for Initial Buckling Analysis of Smart Plates and Beams Using Discrete Layer Kinematics", *International Journal of Solids and Structures*, Vol. 44, pp. 4707-4722 (July 2007).
14. Vel, S. S. and R. C. Batra, "Exact Solution for Rectangular Sandwich Plates with Embedded Piezoelectric Shear Actuators," *AIAA Journal*, Vol. 39, pp. 1363-1373 (July 2001).
15. Deü, J. F. and A. Benjeddou, "Free-Vibration Analysis of Laminated Plates with Embedded Shear-Mode Piezoceramic Layers," *International Journal of Solids and Structures*, Vol. 42, pp. 2059-2088 (April 2005).
16. Zhang, X. D. and C. T. Sun, "Formulation of an Adaptive Sandwich Beam," *Smart Materials and Structures*, Vol. 5, pp. 814-823 (December 1996).
17. Trindade, M. A., A. Benjeddou, and R. Ohayon, "Finite Element Modeling of Hybrid Active-Passive Vibration Damping of Multilayer Piezoelectric Sandwich Beams-Part I: Formulation," *International Journal for Numerical Methods in Engineering*, Vol. 51, pp. 835-854 (July 2001).
18. Raja, S., G. Prathap, and P. K. Sinha, "Active Vibration Control of Composite Sandwich Beams with Piezoelectric Extension-Bending and Shear Actuators," *Smart Materials and Structures*, Vol. 11, pp. 63-71 (Feb 2002).
19. Gu, H., A. Chattopadhyay, J. Li, and X. Zhou, "A Higher Order Temperature Theory for Coupled Thermo-Piezoelectric-Mechanical Modeling of Smart Composites," *International Journal of Solids and Structures*, Vol. 37, pp. 6479-6497 (November 2000).
20. Kim, H.S., X. Zhou, and A. Chattopadhyay, "Interlaminar Stress Analysis of Shell Structures with Piezoelectric Patch Including Thermal Loading," *AIAA Journal*, Vol. 40, pp. 2517-2525 (December 2002).
21. Cho, M. and J. Oh, "A Finite Element Based on Cubic Zig-Zag Plate Theory for the Prediction of Thermo-Electric-Mechanical Behaviors," *International Journal of Solids and Structures*, Vol. 41, pp. 1357-1375 (March 2004).
22. Kapuria, S. and S. D. Kulkarni, "An efficient Quadrilateral Element Element Based on Improved Zigzag Theory for Dynamic Analysis of Hybrid Plates with Electroded Piezoelectric Actuators and Sensors," *Journal of Sound and Vibration*, Vol. 315, pp. 118-145 (August 2008).

23. Plagianakos, T. S. and D. A. Saravanos, "Coupled High-Order Shear Layerwise Analysis of Adaptive Sandwich Composite Beams with Piezoelectric Actuators and Sensors," *AIAA Journal*, Vol. 43, pp. 883-894 (April 2005).
24. Zhen, W. and C. Wanji, "Refined Triangular Element for Laminated Elastic-Piezoelectric Plates," *Composite Structures*, Vol. 78, pp. 129-139 (March 2007).
25. Robbins, D. H. and I. Chopra, "The Effect of Discrete Layer Kinematics on the Global Response of Homogeneous and Composite Plates with Multiple Actuator Pairs," *Journal of Intelligent Material Systems and Structures*, Vol. 18, pp. 235-252 (March 2007).
26. D'Ottavio, M. and B. Kröplin, "An Extension of Reissner Mixed Variational Theorem to Piezoelectric Laminates," *Mechanics of Advanced Materials and Structures*, Vol. 13, pp. 139-150 (March-April 2006).
27. D'Ottavio, M., T. Wallmersperger, and B. Kröplin, "Classical and Advanced Models for Laminated Plates with Piezoelectric Layers Actuated in Shear Mode," *Mechanics of Advanced Materials and Structures*, Vol. 15, pp. 167-181 (2008).
28. Bogner F. K., R. L. Fox, and L. A. Schmidt, "The Generation of Interelement Compatible Stiffness and Mass Matrices by the Use of Interpolation Formulas," *Proceedings. of the Conference. on Matrix Methods in Structural Mechanics, Air Force Institute of Technology, Wright-Patterson Air Force Base,* Ohio US (1965).
29. Plagianakos, T. S. and D. A. Saravanos, "Higher-Order Layerwise Laminate Theory for the Prediction of Interlaminar Shear Stresses in Thick Composite and Sandwich Composite Plates," *Composite Structures*, Vol. 87, pp. 23-35 (January 2009).
30. Plagianakos, T. S. and D. A. Saravanos, "High-Order Layerwise Finite Element for the Damped Free-Vibration Response of Thick Composite and Sandwich Composite Plates," *accepted in the International Journal for Numerical Methods in Engineering*.

APPENDIX

A-1. Formulation of Dicrete Layer Piezoelectric and Electric Permittivity Matrices

The electric permittivity and piezoelectric submatrices of each discrete layer appearing in eqs. (12) and (11), respectively, have the following form:

$$
\begin{aligned}
\boldsymbol{L}_{ll}^{i(k)} &= \frac{h_k}{2}\sum_{m_b^k}^{m_t^k}\int_{\zeta_m^k}^{\zeta_{m+1}^k}\left\{1,\Psi_{1,\zeta_k}^k\zeta_{k,z},\Psi_{2,\zeta_k}^k\zeta_{k,z}\right\}^T\varepsilon_{33}^{m(k)}\left\{1,\Psi_{1,\zeta_k}^k\zeta_{k,z},\Psi_{2,\zeta_k}^k\zeta_{k,z}\right\}d\zeta_k\\
\boldsymbol{L}_{lq}^{i(k)} &= \frac{h_k}{2}\sum_{m_b^k}^{m_t^k}\int_{\zeta_m^k}^{\zeta_{m+1}^k}\left\{1,\Psi_{1,\zeta_k}^k\zeta_{k,z},\Psi_{2,\zeta_k}^k\zeta_{k,z}\right\}^T\varepsilon_{33}^{m(k)}\Psi_{3,\zeta_k}^k\zeta_{k,z}d\zeta_k\\
\boldsymbol{L}_{lc}^{i(k)} &= \frac{h_k}{2}\sum_{m_b^k}^{m_t^k}\int_{\zeta_m^k}^{\zeta_{m+1}^k}\left\{1,\Psi_{1,\zeta_k}^k\zeta_{k,z},\Psi_{2,\zeta_k}^k\zeta_{k,z}\right\}^T\varepsilon_{33}^{m(k)}\Psi_{4,\zeta_k}^k\zeta_{k,z}d\zeta_k\\
\boldsymbol{L}_{qq}^{i(k)} &= \frac{h_k}{2}\sum_{m_b^k}^{m_t^k}\int_{\zeta_m^k}^{\zeta_{m+1}^k}\varepsilon_{33}^{m(k)}\Psi_{3,\zeta_k}^k\Psi_{3,\zeta_k}^k(\zeta_{k,z})^2d\zeta_k\\
\boldsymbol{L}_{qc}^{i(k)} &= \frac{h_k}{2}\sum_{m_b^k}^{m_t^k}\int_{\zeta_m^k}^{\zeta_{m+1}^k}\varepsilon_{33}^{m(k)}\Psi_{3,\zeta_k}^k\Psi_{4,\zeta_k}^k(\zeta_{k,z})^2d\zeta_k\\
\boldsymbol{L}_{cc}^{i(k)} &= \frac{h_k}{2}\sum_{m_b^k}^{m_t^k}\int_{\zeta_m^k}^{\zeta_{m+1}^k}\varepsilon_{33}^{m(k)}\Psi_{4,\zeta_k}^k\Psi_{4,\zeta_k}^k(\zeta_{k,z})^2d\zeta_k
\end{aligned}
\qquad \text{(A1)}
$$

$$
\begin{aligned}
\boldsymbol{P}_{ll}^{\mathrm{i(k)}} &= -\frac{\mathrm{h_k}}{2}\sum_{\mathrm{m_b^k}}^{\mathrm{m_t^k}}\int_{\zeta_{\mathrm{m}}^{\mathrm{k}}}^{\zeta_{\mathrm{m+1}}^{\mathrm{k}}}\left\{\Psi_{1}^{\mathrm{k}},\Psi_{2}^{\mathrm{k}}\right\}^{\mathrm{T}}\mathrm{e}_{3\mathrm{i}}^{\mathrm{m(k)}}\left\{\Psi_{1,\zeta_{\mathrm{k}}}^{\mathrm{k}}\zeta_{\mathrm{k,z}},\Psi_{2,\zeta_{\mathrm{k}}}^{\mathrm{k}}\zeta_{\mathrm{k,z}}\right\}\mathrm{d}\zeta_{\mathrm{k}}\\
\boldsymbol{P}_{lq}^{\mathrm{i(k)}} &= -\frac{\mathrm{h_k}}{2}\sum_{\mathrm{m_b^k}}^{\mathrm{m_t^k}}\int_{\zeta_{\mathrm{m}}^{\mathrm{k}}}^{\zeta_{\mathrm{m+1}}^{\mathrm{k}}}\left\{\Psi_{1}^{\mathrm{k}},\Psi_{2}^{\mathrm{k}}\right\}^{\mathrm{T}}\mathrm{e}_{3\mathrm{i}}^{\mathrm{m(k)}}\Psi_{3,\zeta_{\mathrm{k}}}^{\mathrm{k}}\zeta_{\mathrm{k,z}}\mathrm{d}\zeta_{\mathrm{k}}\\
\boldsymbol{P}_{lc}^{\mathrm{i(k)}} &= -\frac{\mathrm{h_k}}{2}\sum_{\mathrm{m_b^k}}^{\mathrm{m_t^k}}\int_{\zeta_{\mathrm{m}}^{\mathrm{k}}}^{\zeta_{\mathrm{m+1}}^{\mathrm{k}}}\left\{\Psi_{1}^{\mathrm{k}},\Psi_{2}^{\mathrm{k}}\right\}^{\mathrm{T}}\mathrm{e}_{3\mathrm{i}}^{\mathrm{m(k)}}\Psi_{4,\zeta_{\mathrm{k}}}^{\mathrm{k}}\zeta_{\mathrm{k,z}}\mathrm{d}\zeta_{\mathrm{k}}\\
\boldsymbol{P}_{ql}^{\mathrm{i(k)}} &= -\frac{\mathrm{h_k}}{2}\sum_{\mathrm{m_b^k}}^{\mathrm{m_t^k}}\int_{\zeta_{\mathrm{m}}^{\mathrm{k}}}^{\zeta_{\mathrm{m+1}}^{\mathrm{k}}}\Psi_{3}^{\mathrm{k}}\mathrm{e}_{3\mathrm{i}}^{\mathrm{m(k)}}\left\{\Psi_{1,\zeta_{\mathrm{k}}}^{\mathrm{k}}\zeta_{\mathrm{k,z}},\Psi_{2,\zeta_{\mathrm{k}}}^{\mathrm{k}}\zeta_{\mathrm{k,z}}\right\}\mathrm{d}\zeta_{\mathrm{k}}\\
\boldsymbol{P}_{qq}^{\mathrm{i(k)}} &= -\frac{\mathrm{h_k}}{2}\sum_{\mathrm{m_b^k}}^{\mathrm{m_t^k}}\int_{\zeta_{\mathrm{m}}^{\mathrm{k}}}^{\zeta_{\mathrm{m+1}}^{\mathrm{k}}}\Psi_{3}^{\mathrm{k}}\mathrm{e}_{3\mathrm{i}}^{\mathrm{m(k)}}\Psi_{3,\zeta_{\mathrm{k}}}^{\mathrm{k}}\zeta_{\mathrm{k,z}}\mathrm{d}\zeta_{\mathrm{k}}\\
\boldsymbol{P}_{qc}^{\mathrm{i(k)}} &= -\frac{\mathrm{h_k}}{2}\sum_{\mathrm{m_b^k}}^{\mathrm{m_t^k}}\int_{\zeta_{\mathrm{m}}^{\mathrm{k}}}^{\zeta_{\mathrm{m+1}}^{\mathrm{k}}}\Psi_{3}^{\mathrm{k}}\mathrm{e}_{3\mathrm{i}}^{\mathrm{m(k)}}\Psi_{4,\zeta_{\mathrm{k}}}^{\mathrm{k}}\zeta_{\mathrm{k,z}}\mathrm{d}\zeta_{\mathrm{k}}\\
\boldsymbol{P}_{cl}^{\mathrm{i(k)}} &= -\frac{\mathrm{h_k}}{2}\sum_{\mathrm{m_b^k}}^{\mathrm{m_t^k}}\int_{\zeta_{\mathrm{m}}^{\mathrm{k}}}^{\zeta_{\mathrm{m+1}}^{\mathrm{k}}}\Psi_{4}^{\mathrm{k}}\mathrm{e}_{3\mathrm{i}}^{\mathrm{m(k)}}\left\{\Psi_{1,\zeta_{\mathrm{k}}}^{\mathrm{k}}\zeta_{\mathrm{k,z}},\Psi_{2,\zeta_{\mathrm{k}}}^{\mathrm{k}}\zeta_{\mathrm{k,z}}\right\}\mathrm{d}\zeta_{\mathrm{k}}\\
\boldsymbol{P}_{cq}^{\mathrm{i(k)}} &= -\frac{\mathrm{h_k}}{2}\sum_{\mathrm{m_b^k}}^{\mathrm{m_t^k}}\int_{\zeta_{\mathrm{m}}^{\mathrm{k}}}^{\zeta_{\mathrm{m+1}}^{\mathrm{k}}}\Psi_{4}^{\mathrm{k}}\mathrm{e}_{3\mathrm{i}}^{\mathrm{m(k)}}\Psi_{3,\zeta_{\mathrm{k}}}^{\mathrm{k}}\zeta_{\mathrm{k,z}}\mathrm{d}\zeta_{\mathrm{k}}\\
\boldsymbol{P}_{cc}^{\mathrm{i(k)}} &= -\frac{\mathrm{h_k}}{2}\sum_{\mathrm{m_b^k}}^{\mathrm{m_t^k}}\int_{\zeta_{\mathrm{m}}^{\mathrm{k}}}^{\zeta_{\mathrm{m+1}}^{\mathrm{k}}}\Psi_{4}^{\mathrm{k}}\mathrm{e}_{3\mathrm{i}}^{\mathrm{m(k)}}\Psi_{4,\zeta_{\mathrm{k}}}^{\mathrm{k}}\zeta_{\mathrm{k,z}}\mathrm{d}\zeta_{\mathrm{k}}
\end{aligned}
\tag{A2}
$$

where i=1,2 indicates in-plane strains S_1 and S_2, respectively.

A-2. Static Condensation Applied on Discrete Layer Piezoelectric Matrix

The elimination of high-order in-plane elastic field terms arising from derivation of eqs. (14) requires partitioning of the piezoelectric matrix of each discrete layer as,

$$
\left[\boldsymbol{P}^{\mathrm{k}}\right]=\begin{bmatrix}\boldsymbol{P}_{1}^{\mathrm{k}}\\ \boldsymbol{P}_{2}^{\mathrm{k}}\end{bmatrix}
\tag{A3}
$$

The reduced piezoelectric matrix of each discrete layer is given by,

$$
\left[\boldsymbol{P}_{\mathrm{r}}^{\mathrm{k}}\right]=\begin{bmatrix}\left[\Pi_{\mathrm{p}}^{(1,\mathrm{k})}\right]\\ \left[\Pi_{\mathrm{p}}^{(2,\mathrm{k})}\right]\\ \vdots\\ \left[\Pi_{\mathrm{p}}^{(\mathrm{k},\mathrm{k})}\right]\end{bmatrix}
\tag{A4}
$$

where the submatrices $[\Pi_{\mathrm{p}}]$ are given by,

$$
\begin{aligned}
\left[\Pi_{\mathrm{p}}^{(\mathrm{k},\mathrm{k})}\right]&=\left[\boldsymbol{P}_{1}^{\mathrm{k}}\right]+\left[\tilde{\Lambda}^{(\mathrm{k},\mathrm{k})}\right]^{\mathrm{T}}\left[\boldsymbol{P}_{2}^{\mathrm{k}}\right]\\
\left[\Pi_{\mathrm{p}}^{(l,\mathrm{k})}\right]&=\left[\tilde{\Lambda}^{(\mathrm{k},l)}\right]^{\mathrm{T}}\left[\boldsymbol{P}_{2}^{\mathrm{k}}\right]
\end{aligned}
\tag{A5}
$$

A-3. Formulation of Reduced Laminate Piezoelectric Matrix

The reduced piezoelectric matrix of the laminate is built from all discrete layers as,

$$\left[\boldsymbol{P}_{\mathrm{r}}^{\mathrm{L}}\right]=\begin{bmatrix}\left[\Pi_{\mathrm{p}}^{(1,1)}\right] & \left[\Pi_{\mathrm{p}}^{(1,2)}\right] & \cdots & \left[\Pi_{\mathrm{p}}^{*(1,\mathrm{n})}\right]\\ & \left[\Pi_{\mathrm{p}}^{(2,2)}\right] & \cdots & \left[\Pi_{\mathrm{p}}^{*(2,\mathrm{n})}\right]\\ & & & \vdots\\ & & \cdots & \left[\Pi_{\mathrm{p}}^{*(\mathrm{n},\mathrm{n})}\right]\end{bmatrix} \tag{A6}$$

where the asterisk indicates different dimensions due to elimination of the derivatives of all high-order terms $\alpha_{\mathrm{x}}^{\mathrm{n}},\alpha_{\mathrm{y}}^{\mathrm{n}},\lambda_{\mathrm{x}}^{\mathrm{n}},\lambda_{\mathrm{y}}^{\mathrm{n}}$ of the upper-surface discrete layer.